

# How can the Vicsek model be applied and modified to explore the phase transitions and milling states of active matter systems?

Robert J. Smith

April 2023

## Abstract

In this paper we explore the phase transition of the Vicsek model, a simple model used for simulating collective motion in active matter systems. Computational methods and a real-time simulation application were developed to analyze the effect of noise and density on the phase transition, producing results consistent with existing literature. Modifications to the model are made to study milling (vortex) states commonly found in nature. Improvements to the existing vortex detection algorithm are given and a newly developed vortex detection algorithm is compared with existing methods. These techniques are used to study the milling state producing results consistent with the literature. Though these models are minimal, they provide a foundation for further exploration into more realistic models. The real-time simulation and vortex detection algorithms developed could be useful in teaching and understanding collective motion of other active matter models.



*A Report Submitted In Partial Fulfilment  
Of The Requirements For The Degree Of*

Master of Natural Science, MSci (Hons)  
University of Durham

*Supervised by Dr Stephen Wrathmall*

# Table of Contents

<b>1</b>	<b>Introduction</b>	<b>3</b>
<b>2</b>	<b>Vicsek Model</b>	<b>4</b>
2.1	Theory . . . . .	4
2.2	Phenomenology . . . . .	5
2.3	Limiting Cases . . . . .	6
<b>3</b>	<b>Computational methods</b>	<b>7</b>
3.1	Numerical Convergence . . . . .	7
3.2	Performance Improvement . . . . .	8
3.3	Real-Time Simulation . . . . .	9
<b>4</b>	<b>Vicsek Phase Transition</b>	<b>10</b>
4.1	Results . . . . .	10
4.2	Discussion . . . . .	12
<b>5</b>	<b>Milling Modification</b>	<b>14</b>
5.1	Theory . . . . .	14
5.2	Phenomenology . . . . .	14
<b>6</b>	<b>Vortex Detection</b>	<b>15</b>
6.1	Clustering . . . . .	15
6.2	Vortex Criteria . . . . .	17
6.3	Problems With Existing Methods . . . . .	17
6.4	New Vortex Detection Algorithm . . . . .	19
<b>7</b>	<b>Milling Experiments</b>	<b>20</b>
7.1	Results . . . . .	20
7.2	Discussion . . . . .	23
<b>8</b>	<b>Conclusions</b>	<b>24</b>
<b>9</b>	<b>Future work</b>	<b>24</b>
	<b>References</b>	<b>25</b>

## 1. INTRODUCTION

The study of collective motion in active matter system presents a fascinating, multidisciplinary and rapidly developing area of research. Active matter consists of the study of large numbers of self propelling agents or particles [1]. Collective motion is the emergence of large scale moving structures generated from locally interacting agents. Examples of collective motion in active matter can be found in Fig. 1. These natural phenomena can be observed at all scales from flocking birds and schools of fish to ant and bacterial colonies.

The motion of these self propelling agents can be modelled as violating conservation of momentum, however the emerging systems generated can share many similarities with equilibrium systems studied in statistical physics [2]. The universal nature of these phenomena at all scales suggests that minimal models can be used to explore the universal features of the emergence observed. The conventional model used to study such phenomena is the Vicsek model [3]. This is one of the simplest models displaying a transition to collective motion and is an important model to build intuition about collective phenomena.

In this paper we explore the phase transition present in the Vicsek model which has been of historic controversy [4]. We present the basic phenomenology of the model followed by computational methods for the production of large simulations. An application to simulate the model in real time is developed and used to explain the trends observed in the phase transition. The application is used to visually confirm the first order nature of the phase transition by reproducing the band structure of the liquid-gas phase transition [5].

We modify the Vicsek model to study the collective motion of milling (vortex) states commonly found in nature as seen in Fig. 1(b) and 1(c) [6]. Problems in the existing vortex detection algorithm for real time tracking of vortex formation are presented and we provide a simple generalisation of the algorithm to increase the reliability of the current implementation. Furthermore, we provide a new vortex detection algorithm and compare it to existing methods. This new algorithm is used to replicate the general findings of the milling model and we discuss the trends observed in the milling regime.

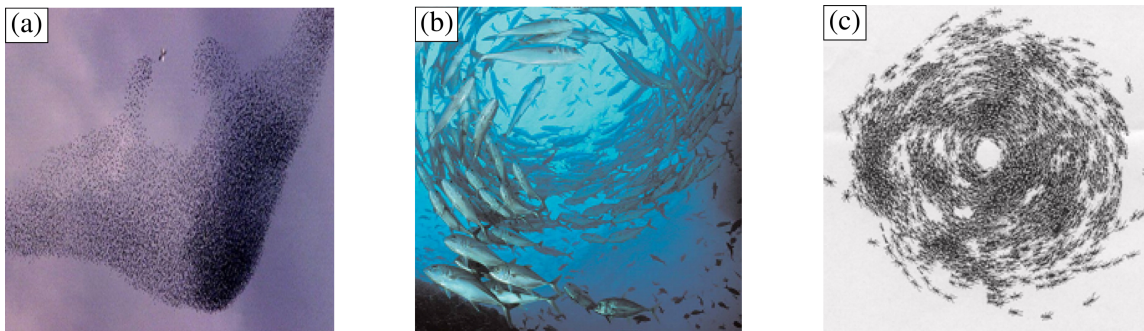


**FIG. 1:** Examples of collective motion in nature: (a) The flocking formation of starlings (b) Fish in a milling state (c) Rotating colony of army ants. [Figure adapted from [7]]

## 2. VICSEK MODEL

### 2.1. Theory

The Vicsek model consists of  $N$  number of particles in a 2D square cell of dimensions  $L \times L$  with periodic boundary conditions. Initially, the particles have random positions and orientations of velocity with the magnitude of the velocity  $v$  held constant.

We evolve the model using a time step of  $\Delta t = 1$ . The position of every particle in the system is updated every time step. The position of the  $i$ -th particle  $\mathbf{x}_i$  is updated as

$$\mathbf{x}_i(t+1) = \mathbf{x}_i(t) + \mathbf{v}_i(t)\Delta t \quad (1)$$

where  $\mathbf{v}_i$  is the velocity of the  $i$ -th particle.

Once all particles have moved position, we update the velocity by updating the orientation of the particles. The angle  $\theta$  (defined clockwise from the y-axis) for each particle is updated as

$$\theta(t+1) = \langle \theta(t) \rangle_r + \Delta\theta \quad (2)$$

where  $\langle \theta(t) \rangle_r$  is the average orientation of all particles within the interaction circle. The interaction circle is defined as the circle formed from the interaction radius  $r = 1$  centered on the position of the particle. Here  $\Delta\theta$  is a random number distributed with uniform probability in the interval  $[-\eta/2, \eta/2]$  where  $\eta \in [0, 2\pi]$  is a noise term analogous to the temperature in statistical physics. It is convenient to combine the linear length and the number of particles into a density given as

$$\rho = \frac{N}{(L \times L)} \quad (3)$$

. A visual representation of an implementation of the velocity update rule for a single particle is given in Fig. 2.

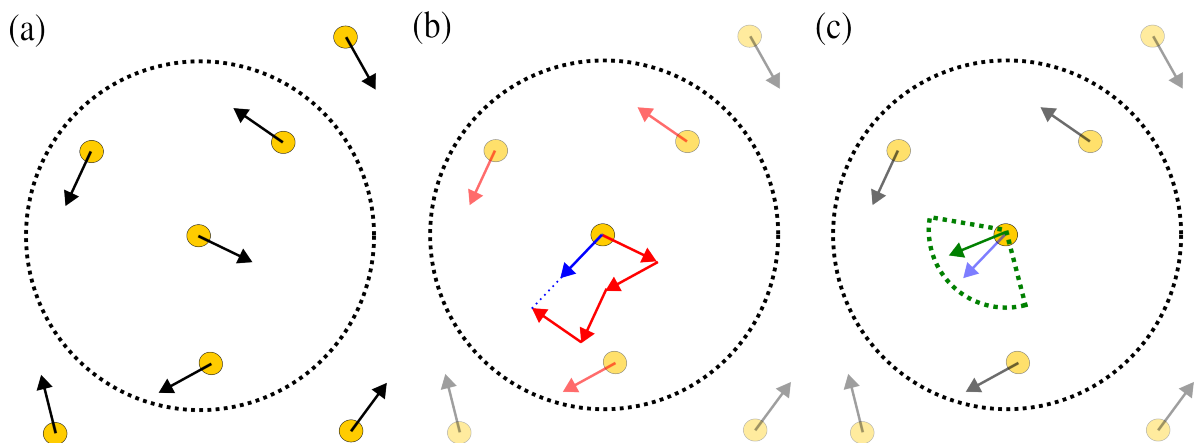


**FIG. 2:** The velocity update rule for a single particle in the Vicsek model: (a) Velocity updates only consider particles inside the interaction circle (black dotted circle) (b) The new velocity (blue) is the normalised sum of all velocities in the interaction radius (red) (c) The final velocity (green) is obtained by rotating the vector (blue) in (b) by a random angle taken from a uniform distribution  $[-\eta/2, \eta/2]$ .

## 2.2. Phenomenology

We have three parameters controlling the behaviour of the model: speed  $v$ , number of particles  $N$  and density  $\rho$ . In this model, momentum is not conserved which leads to interesting far from equilibrium phenomena. As discovered in the original Vicsek paper (Ref. [3]), we observe different regimes by varying the noise and number of particles with all other parameters held constant. We illustrate the behaviour under these conditions in Fig. 3, where each square shows a snapshot of the system after 100 time steps. The previous 20 steps are highlighted in colour and the velocities are shown (as black arrows).

In both high noise regimes, each individual particle evolves with diffusion-like behaviour with the effect of the interaction between particles being small. In the low density low noise regime we observe a few small clusters of particles moving together in the same direction. The most striking result is the high density low noise regime in which all particles collectively move together in the same direction.

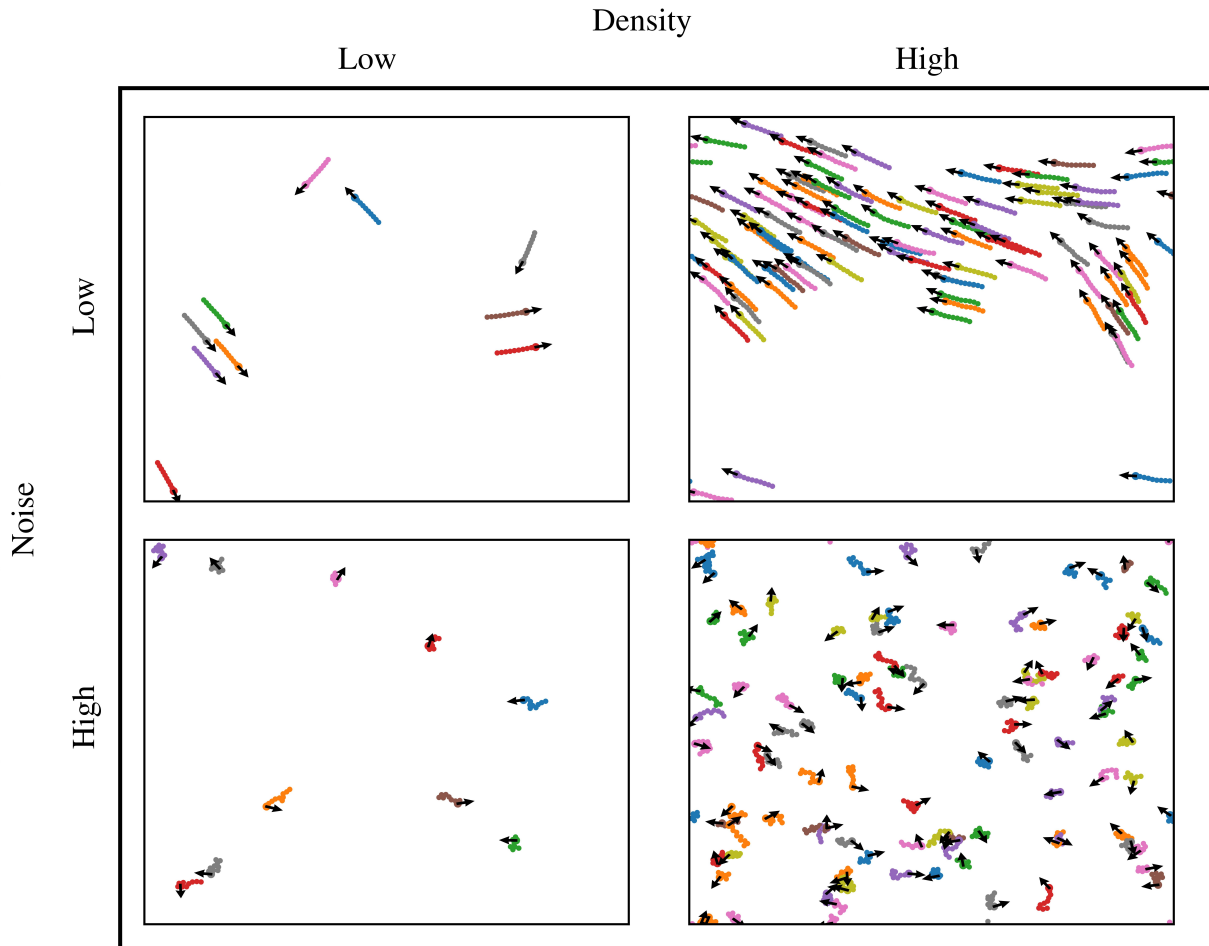


**FIG. 3:** Snapshots of the Vicsek model after 100 time steps for different density and noise regimes. The previous 20 steps are highlighted in color with the black arrows indicate the velocities of each particle.

Simulations were performed with  $v = 0.3$ ,  $L = 10$ , for noise (low = 0.1 high = 5.0) and density (low = 0.1 high = 1.0).

In this case, the particles have transitioned from a disordered initial state to an ordered collective motion state, breaking the rotational symmetry found in the initial configuration. The breaking of this symmetry suggests that the system has undergone a phase transition [8].

An order parameter can be used to track the change from a disordered collection to an ordered collection of particles [9]. The convention when studying the Vicsek model is to use the absolute value of the average normalised velocity, in the rest of this paper we call this the normalised velocity  $v_a$ . This is calculated as

$$v_a = \frac{1}{Nv} \left| \sum_{i=1}^N \{v_i\} \right| \quad (4)$$

and has value 0 in the disordered state where many particles move with completely random velocities and a value of 1 in the ordered state where all particles are aligned in the same direction.

### 2.3. Limiting Cases

In this paper we use speeds ( $0.003 \leq v \leq 0.3$ ) such that neighbouring particles can interact for multiple time steps and particles move fast enough such that the configuration of the system changes after a reasonable number of steps. Analogies to statistical physics can be made in the limits of the model. In the limit when  $v \rightarrow 0$  for systems with large density the model behaves as an off-lattice classical XY ferromagnet model where noise acts like temperature [10]. For  $v \rightarrow \infty$  we get complete mixing between two time steps which corresponds to the mean field behaviour of a ferromagnet [3].

The reproduction of the XY model from the Vicsek model is illustrated in Fig. 4. For large noise we have the particle velocities randomly oriented as shown in Fig. 4(a). This is analogous to particles in a ferromagnet having randomly aligned spins at high temperatures. Below a critical noise value we get the formation of regions of aligned velocities as displayed in Fig. 4(b). This is analogous to spins in a ferromagnet below the Curie temperature aligning to form magnetic domains.

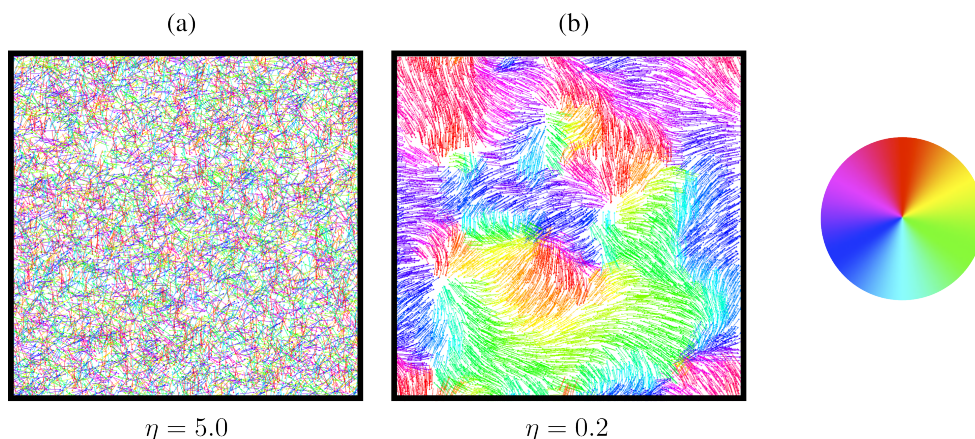


**FIG. 4:** Vicsek model in the limit  $v \rightarrow 0$ . Simulations were performed at  $v = 0.1$ ,  $L = 25$ ,  $N = 10000$ .

(a) High noise simulation showing randomly oriented particles. (b) Low noise simulation showing regions of aligned particles. The colour of a particle is determined by mapping the orientation onto the colour wheel shown.

### 3. COMPUTATIONAL METHODS

#### 3.1. Numerical Convergence

In studying phase transitions we are interested in computing the asymptotic (large  $N$  and long time) properties of the model. When performing large numerical simulations it is beneficial to minimise the number of calculations performed once the system has reached a steady state. An example of how one might calculate the long term behaviour of the order parameter is shown in Fig. 5. In this experiment we are measuring how the value of the order parameter changes for varying noise and number of particles.

Due to the normalised velocity having large variance across time we consider the moving average of the normalised velocity which converges to a singular value. To verify convergence we can construct a difference range  $\Delta$  that represents the difference between the largest and smallest moving average values in the previous 10 time steps.

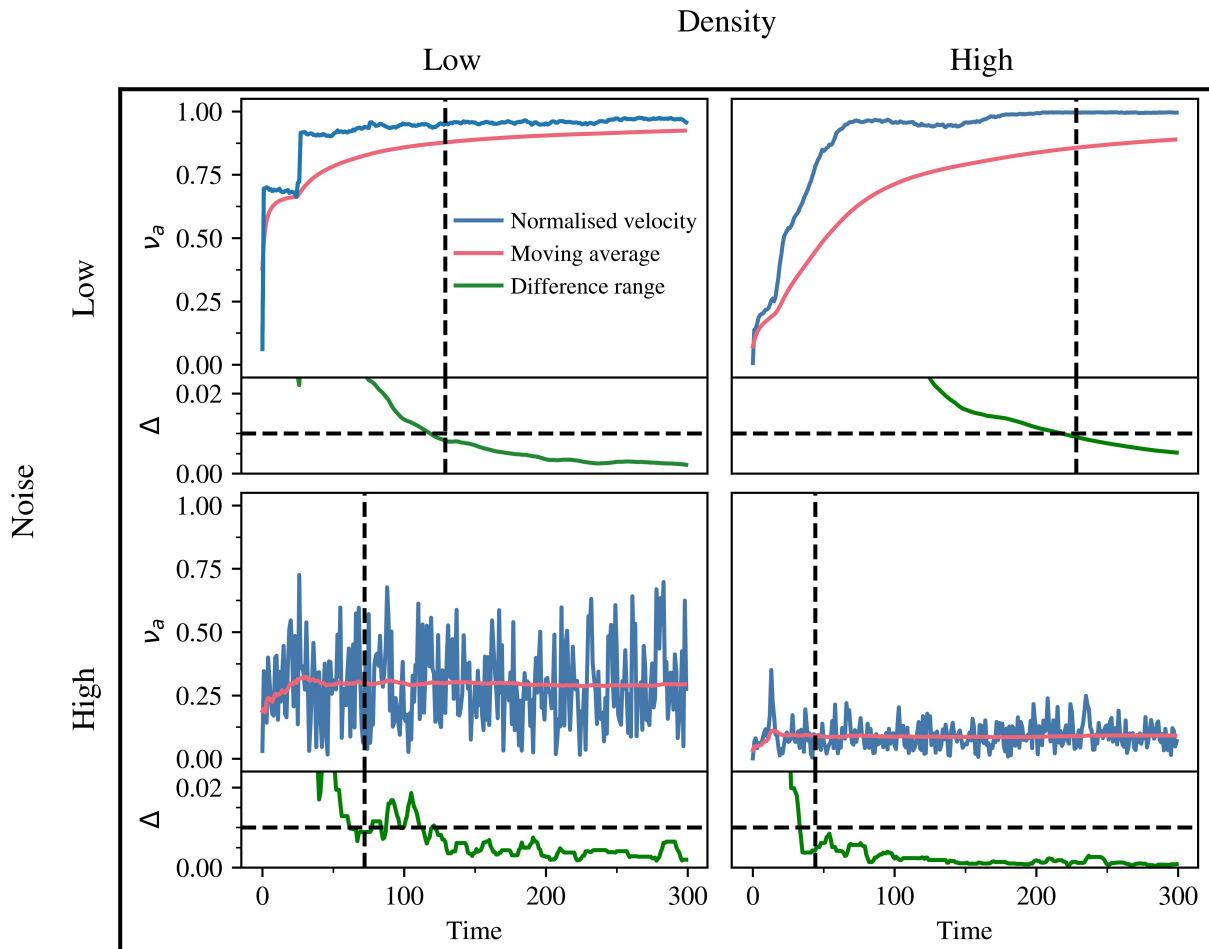


**FIG. 5:** A method to calculate convergence of a system of fixed linear size. The difference range  $\Delta$  is a custom convergence criteria (see text). The moving average is computed from the last 10 time steps of the normalised velocity. The horizontal dashed line shows the 0.01 convergence threshold and the vertical dashed line shows the convergence point. Simulations were performed with  $v = 0.3$ ,  $L = 10$ , for noise (low = 0.1 high = 5.0) and density (low = 0.1 high=1.0).

Empirically this was found to give a good estimate of the convergence when the difference range dropped under 0.01 for 10 consecutive time steps. Based on this criteria the convergence point is marked with the vertical black dashed line in Fig. 5.

Although this criteria is sufficient in the given range of parameters, it fails as linear length is increased. The number of previous steps considered in the calculation of  $\Delta$  needs to increase with system size to guarantee convergence. In most experiments we cannot easily construct a convergence criteria. The more robust way of ascertaining convergence is to plot a visualisation of the desired statistic across time for the slowest converging parameters. One can then visually check where the value settles and then run all experiments to that time step. This is likely to give convergence of all runs in the experiment.

To explain the results found in Fig. 5 we can compare with what we found in Fig. 3. The low noise regimes have smaller variance in the normalised velocity than the high noise regimes as the high noise causes large changes of the orientations at each step preventing large scale alignment. The high noise high density regime has lower variance than the high noise low density regime. This is due to the lower density regime having a higher chance of spontaneous alignment between a significant proportion of the particles. The larger number of particles in the high density regime reduces the chance of large spontaneous alignment, thus causing the normalised velocity to be closer to 0, with the lower variance resulting in faster convergence. The low density low noise regime has longer convergence as the time between collisions in the low density regime is larger. We notice the collective motion regime has the largest convergence time due to the complex interactions between collections of clustered particles such that they all orientate to the same direction.

### 3.2. Performance Improvement

Our initial simulations were performed using Python, a powerful all-purpose programming language capable of rapid prototyping. Despite its benefits, Python is not a fast programming language [11]. We required a new programming language suitable for large scale particle simulations.

The Rust programming language is designed for performance and memory safety. It has speeds comparable to C and FORTRAN and its novel memory management system allows for safe executing fast code [11]. These properties have ensured its place as a highly regarded language for developers [12]. Therefore, Rust was chosen as the programming language for the simulation.

In considering Eq. 2, a simple approach to calculate which particles are within the interaction radius is to check the distance between the updating particle and all other particles in the simulation. Although simple to implement, this calculation scales with the number of particles as order  $\mathcal{O}(N^2)$  meaning the performance of the program is proportional to the square of the number of particles [10]. This approach is very computationally expensive at the scales we wish to observe.

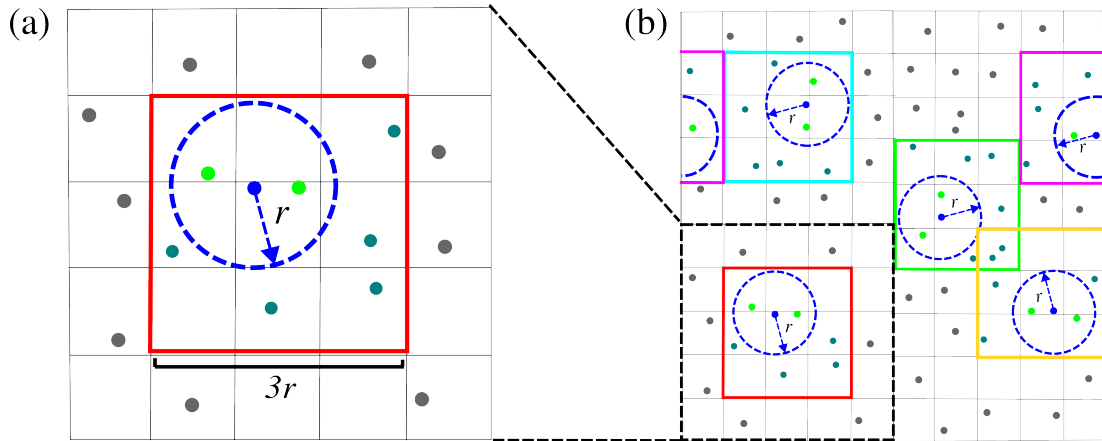


**FIG. 6:** Computational methods to increase performance of the Vicsek model. (a) Domain decomposition to reduce number of distance calculations (see text) (b) Parallel velocity updates on different coloured grids.

A better approach commonly used in molecular dynamics simulations is shown in Fig. 6(a) [13]. We decompose the simulation area into smaller grids of length 1. The interaction radius is  $r = 1$ , hence we only need to consider the particles in the  $3 \times 3$  grid surrounding the current particle (blue) as there is no possibility of interacting with particles outside of this range (gray). Distance has to be computed to the green particles which are dull green if they are outside the interaction circle and light green if they are inside. At a fixed density, the mean number of particles found within each small grid remains constant, as an increase in number of particles corresponds to an increase in total area at fixed density. Hence the number of computations performed per update step scales as  $\mathcal{O}(N)$  allowing for a larger number of particles to be simulated [10].

We can improve performance further by performing updates in parallel. An example of this is shown in Fig. 6(b). Each different coloured  $3 \times 3$  grid is executed on a separate CPU and therefore we can perform multiple calculations simultaneously. The velocity of the particles do not change until all velocity updates have been calculated allowing for overlapping grids in the calculations.

In Python - before applying these computational methods - simulations of 1000 particles updating for 30 time steps required one minute of computation time. Using Rust and the discussed techniques, simulations of 10000 particles can update 30 time steps every second. These techniques allow us to perform faster calculations on larger systems.

### 3.3. Real-Time Simulation

To visualise the model, a simulation application was built in Rust using the 2D games engine framework *ggez* [14]. The flow diagram of the code used in generating the simulation is shown in Fig. 7(a). The order parameters and additional statistics are computed in the measure statistics step. The rendering of the particles to the screen occurs in the update sprites step. Each particle is a game sprite which gets batched together for rendering performance. A game engine was used as standard graphing libraries were unable to update parameters in real time based on inputs by the user.

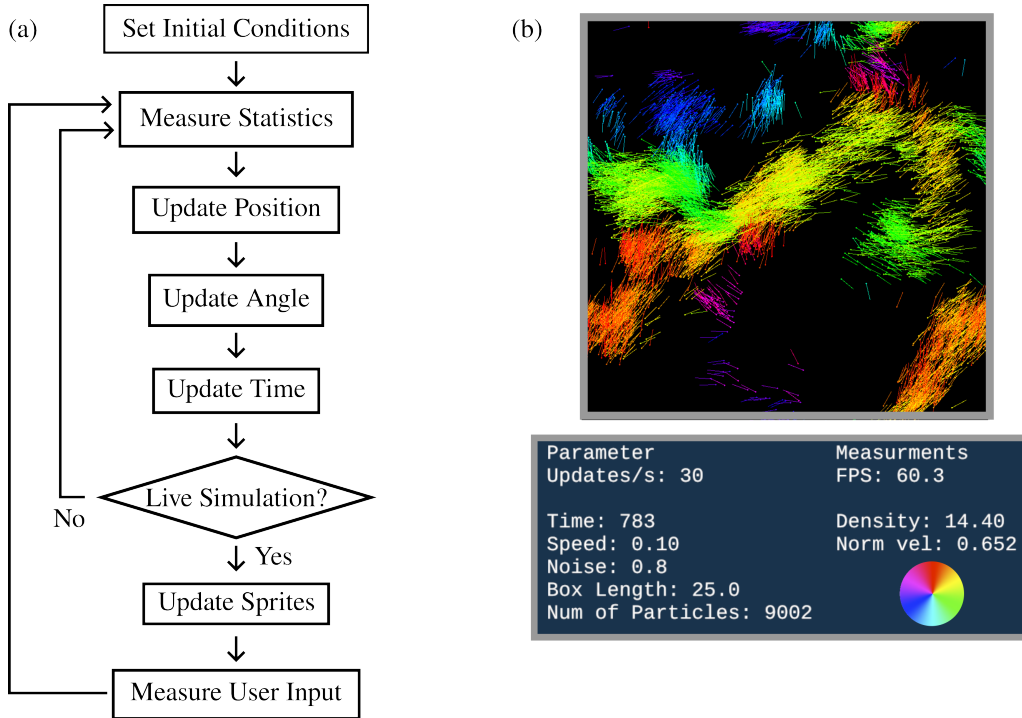


**FIG. 7:** (a) Flow diagram of code used in the live simulation (b) Screenshot of the simulation software. The colour of a particle is determined by mapping the orientation onto the colour wheel shown.

A screenshot of a simulation alongside its parameters is shown in Fig. 7(b). The ability to vary parameters in real time allows intuition to be built about the dynamics of the system. It allows for fast exploration of different regimes and quick intuition tests to be conducted. Visualisation allowed for consistency checks of the code. Changes to the code could be checked against the expected behaviour, thus increasing the reliability of the code.

## 4. VICSEK PHASE TRANSITION

### 4.1. Results

In the Vicsek model, the long time averaged value of the normalised velocity depends on the noise and density of the system. We consider how the normalised velocity changes with noise in Fig. 8. This is a reproduction of the experiment carried out in the original Vicsek paper [3]. The original data was extracted from the paper via the *g3data* program [15]. The exact value of the parameters were not given in the original paper however we estimated that the simulations were performed at speed  $v = 0.3$  and density  $\rho = 4.0$ . Simulations were performed for 10000 time steps with the final 1000 steps being used to calculate the average of the normalised velocity. These experiments were repeated 5 times to attain uncertainties.

We observe that the system transitions from a disordered state at high noise to an ordered state at low noise which matches what we observed in Fig. 3. We have visual agreement for low numbers of particles however there are large discrepancies for the  $N = 4000$  and  $N = 10000$  case. This is shown clearly by the peaks in the residual plot. We performed our estimation of the parameter values used in this paper by matching the results of experiments for low numbers of particles, which is a possible explanation for the discrepancy at large particle numbers.

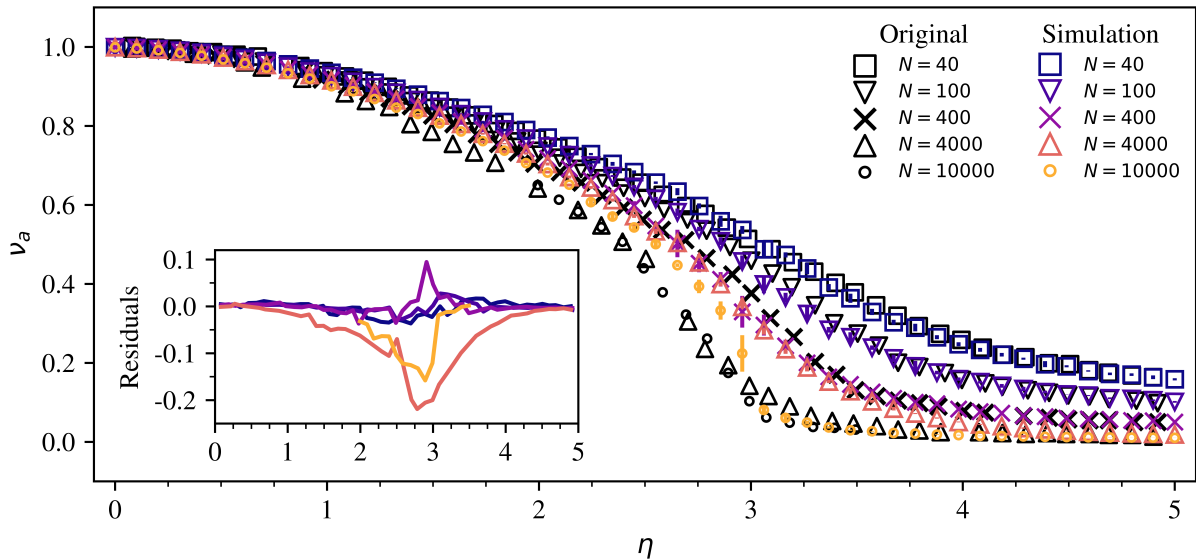


**FIG. 8:** Normalised velocity vs noise for a system with  $v = 0.3$ ,  $\rho = 4.0$ . Black markers represent results from the original Vicsek paper, coloured markers represent results found in this paper.

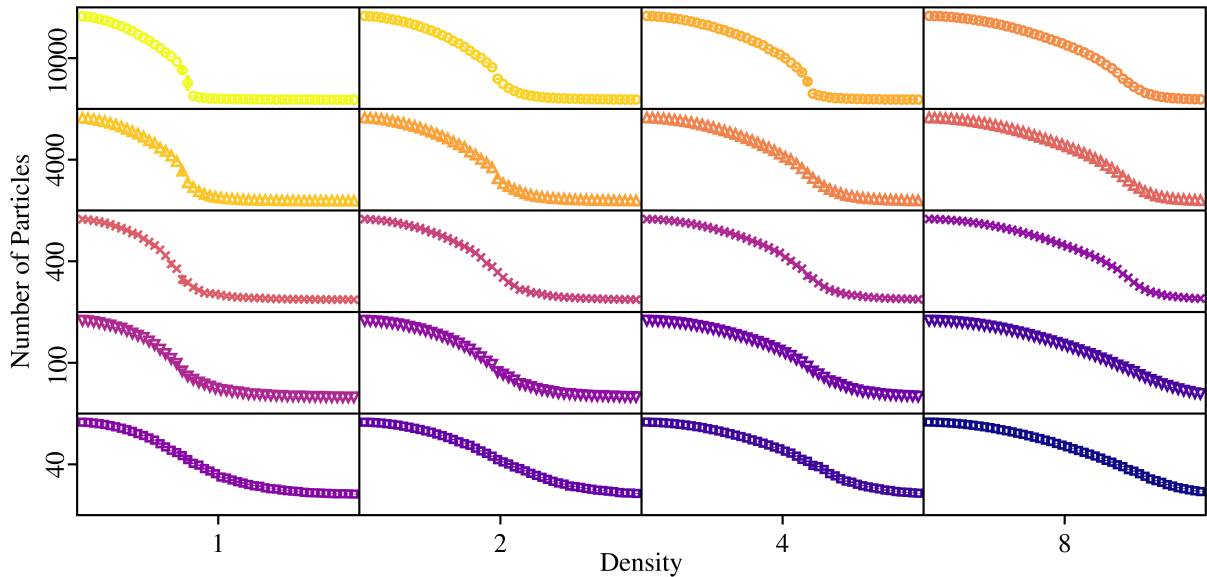


**FIG. 9:** Sub-graphs of normalised velocity vs noise (with scale of Fig. 8) for varying number of particles and density for  $v = 0.3$ . Hotter colours represent systems with larger box lengths.

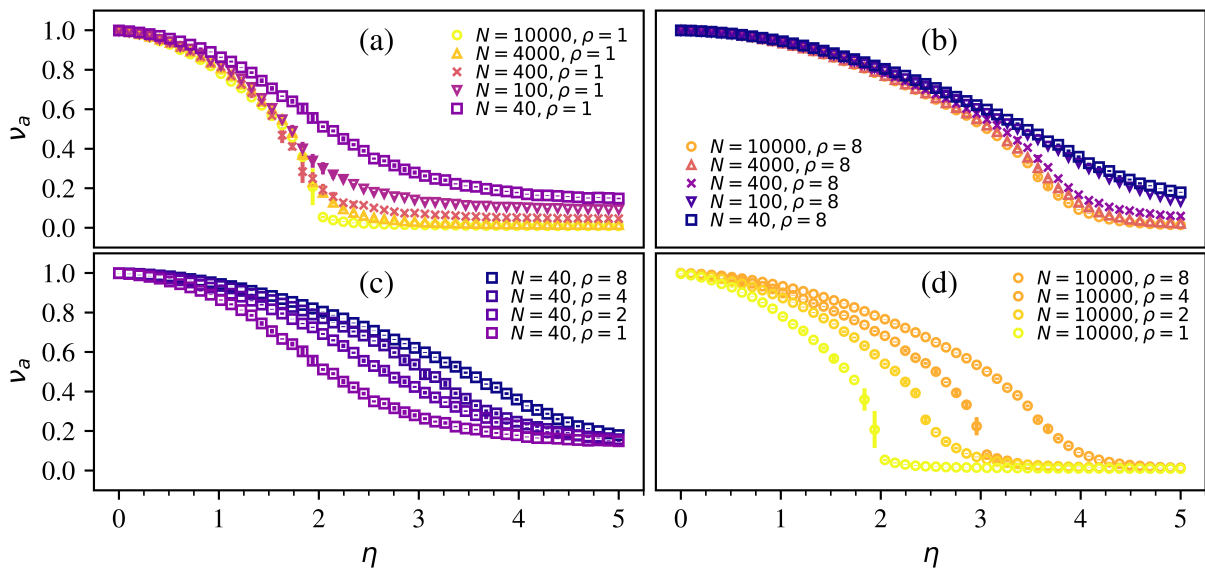


**FIG. 10:** Comparison of the normalised velocity vs noise for different ranges of Fig. 9.

A more comprehensive set of simulations across the parameter range is given in Fig. 9. Each sub-graph has the same scale as Fig.8. The hotter colour represents larger box lengths. An increase in density at a fixed number of particles reduces the sharpness of the curve and shifts the steepest part of the transition to higher noise values. Decreasing the number of particles in the simulation for fixed density reduces the sharpness of the transition and increases the normalised velocity value at high noises.

We consider the extreme values of Fig. 9 in Fig. 10. Comparing Fig 10(a) and 10(b) shows that decreasing the number of particles at fixed density causes the transition to be less sharp and shifts the steepest part of the transition to higher noise values and that a smaller linear box size always shifts the transition to higher noise values.

Comparing Fig 10(c) and 10(d) we note again that values with the larger box length have sharper transitions and that lower particle numbers have greater normalised velocity at high noises. We also observe that the distribution of lines at high numbers of particles are spread out and the largest uncertainties of normalised velocities occur at low densities and large box size.

#### 4.2. Discussion

The observed trends can be summarised and explained as follows.

- *The system transitions from disorder to order as we decrease noise.* Information is required to propagate through the whole system to obtain alignment. The alignment term in Eq. 2 introduces information transfer, however the random noise term counteracts this effect. Hence we would expect a decrease in noise to lead to alignment between particles.
- *Increasing density for a fixed number of particles reduces the sharpness of the transition and shifts the steepest part of transition to higher noises.* This is most obvious in Fig. 10(d). The decrease in box length causes there to be a smaller distance between particles, allowing information to propagate more effectively. This means the system can withstand more noise hence the sharp transition being shifted to higher noise. The smaller distance also increases the stability of the transition allowing it to occur over a wider range of values, decreasing the sharpness of the transition. This allows the model to undergo the transition at fixed noise by increasing the density of the system.
- *Decreasing the number of particles at a fixed density reduces the sharpness and moves the transition to higher noises.* This is most obvious in Fig. 10(a). Although there are fewer particles, the box length has decreased. The particles can travel further in a given time step, allowing more efficient information transfer. Using the argument above we decrease sharpness and shift the transition to higher noises.
- *Simulations with a low number of particles have increased normalised velocity value at high noise.* This is most obvious in Fig. 10(b). This can be explained by the higher normalised velocity variance due to spontaneous alignment (see argument regarding Fig. 5).
- *The largest uncertainties come from simulations with a large number of particles at low densities.* This is most obvious in Fig. 10(d). The particles have to travel the largest distance to transmit information, implying slow convergence, leading to larger errors.

- *The distribution of lines at a high number of particles are more spread out.* This is most obvious in Fig. 10(d). This might be due to the presence of more particles causing the behaviour of the system to be more prominent. The true behaviour of the phase transition is only obtained in the thermodynamic limit for  $L \rightarrow \infty$  and  $N \rightarrow \infty$ .

The continuous change of the order parameter in all experiments would suggest a continuous phase transition. If this was true, one could compute critical exponents of the transition as was done when this transition was first discovered [3]. However, recent evidence has shown that the phase transition is discontinuous and that therefore this analysis is invalid. The discontinuity is observed when considering much larger system configurations [16]. Due to the long run time of these experiments we could not replicate this result during the time frame of the investigation.

The true nature of this phase transition is like that of a liquid-gas phase transition [5]. An illustration of the different regimes is shown in Fig. 11. At the onset of order we get bands of collectively moving particles in a background of diffusing particles. These bands are not observed until around 10,000 particles and arise due to the feedback loop of local alignment causing areas of higher density and increasing the efficiency of alignment [5]. Although we cannot show the discontinuity of the transition we observe formation of these bands for large simulations. The large difference between this phase diagram and liquid-gas phase diagram is the fact that there is no access to the super critical regime.

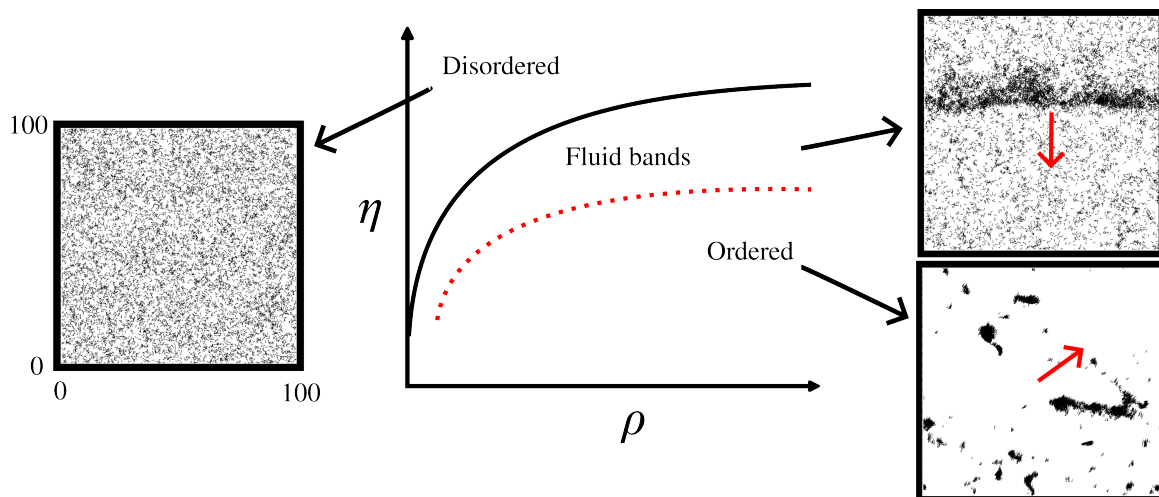


**FIG. 11:** The phase diagram of the Vicsek model for large system size. For parameters:  $v = 0.5$ ,  $\rho = 1.0$ ,  $N = 10000$ . Ordered  $\eta = 0.0$ , Fluid bands  $\eta = 2.0$ , Disordered  $\eta = 4.0$ . The black line represent the order-disorder transition and red dotted line is the transition between bands and flocks.

The red arrows show direction of travel.

## 5. MILLING MODIFICATION

### 5.1. Theory

Following the work of A. Costanzo and C. K. Hemelrijk (Ref. [6]) we can modify the Vicsek model to produce milling (vortex) effects. The first modification is to introduce a field of view for each particle  $\phi$ . This modifies the alignment term such that alignment occurs only if neighbouring particles are within the interaction circle and within the field of view of the particle, an illustration of this is shown in Fig. 12.

Furthermore, we introduce a maximum angular velocity  $\omega \in [0^\circ, 180^\circ]$ . In the Vicsek model each particle can rotate by an arbitrary angle at each velocity update step. This parameter is the limit of the rotation per update step. These two changes modify Eq. 2 to

$$\theta(t+1) = \begin{cases} \langle \theta(t) \rangle_{r,\phi} + \Delta\theta & \text{for } |\Delta\Theta| < \omega \\ \theta(t) + \omega + \Delta\theta & \text{for } \Delta\Theta \geq \omega \\ \theta(t) - \omega + \Delta\theta & \text{for } \Delta\Theta \leq -\omega \end{cases} \quad (5)$$

where  $\langle \theta(t) \rangle_{r,\phi}$  is the average direction of the velocities of all the particles within the interaction circle and field of view and  $\Delta\Theta$  is the difference in orientation between the current orientation of the particle and the average of all interacting particles.

### 5.2. Phenomenology

The effect of these two modifications can be observed in Fig. 13. The emergence of milling in Fig. 13(c) is attributed to each particle having a reduced field of view, constraining its alignment to particles ahead of it. Further the maximum angular velocity prevents immediate alignment with these particles which leads to stable formation of vortices. We note in the modified model the original Vicsek model can be reproduced by setting  $\phi = 360^\circ$  and  $\omega = 180^\circ$ .

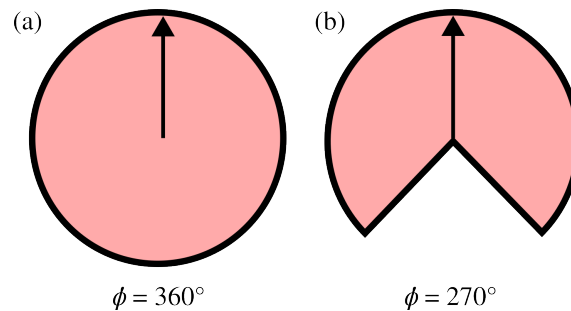


**FIG. 12:** Field of view modification to the interaction circle. The interaction area is given in red. The black arrow represents direction of velocity. (a) Shows total field of view as in the original Vicsek model (b) Shows an example of a limited field of view.

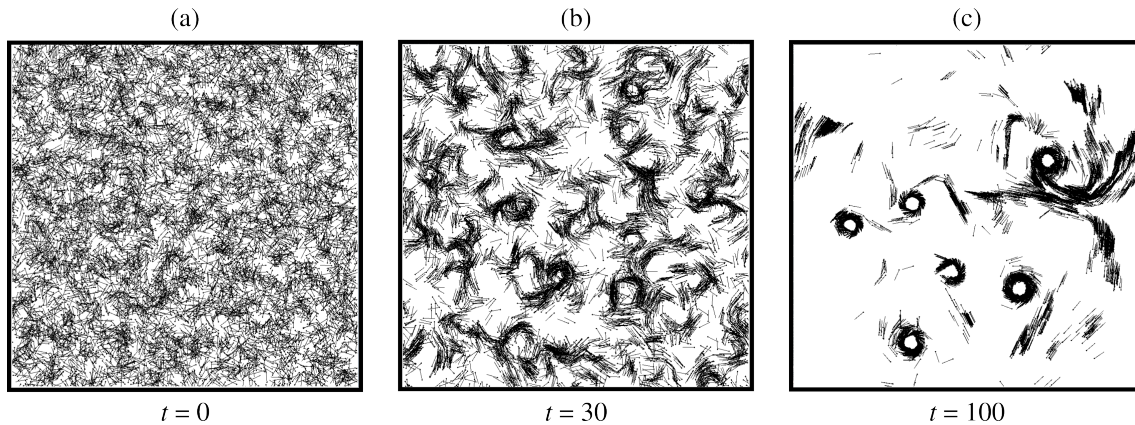


**FIG. 13:** Example of milling formation for  $v = 0.1$ ,  $L = 30$ ,  $N = 10000$ ,  $\eta = 0.0$ ,  $\phi = 180^\circ$ ,  $\omega = 10^\circ$ .  
 (a) Initial configuration (b) The initial formation of clusters (c) Stable milling configuration.

## 6. VORTEX DETECTION

### 6.1. Clustering

To ascertain when a vortex has been created we introduce a generalisation of the algorithm used in the work of A. Costanzo and C. K. Hemelrijk (which we henceforth call the milling paper) [6]. This approach relies on the clustering algorithm DBSCAN (Density-Based Spatial Clustering of Applications with Noise) [17]. This algorithm is designed to classify complex clusters.

A visual guide to explain this algorithm is given in Fig. 14. This algorithm has two tuning parameters: the minimum sample of points  $\text{minPts}$  and the exploratory radius  $\epsilon$ . For each particle we count the total number of particles found within the circle formed by the exploratory radius 14(a). If this number is greater than the minimum sample  $\text{minPts}$  its classified as a core point, otherwise it is classified as a non-core point 14(b). Then a randomly selected core point becomes a cluster. This cluster propagates out to all other connected core points 14(c), this is repeated until all core points are classified. Each non-core point is selected in turn, if it is connected to a core point then it inherits the label of that cluster, if it does not neighbour any cluster then it forms a noise point 14(d). In this way we classify all particles in the simulation into clusters and noise points.

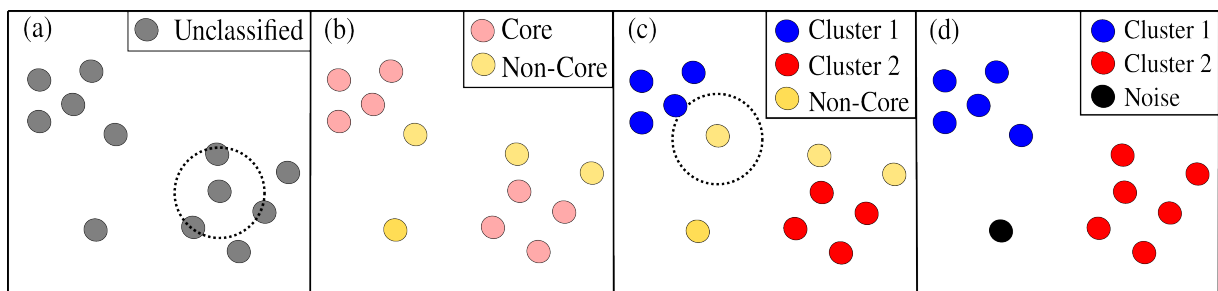


**FIG. 14:** The four main steps of the DBSCAN algorithm for identifying clusters for  $\text{minPts} = 2$ . The full explanation of the algorithm can be found in main body of the text.

It is insightful to compare how the order parameter and clustering statistics change across the phase transition of the original Vicsek model. The results of this are shown in Fig. 15. As previously observed the normalised velocity increases from 0 to 1 as the particles transition to collective motion. We observe that the number of clusters decreases as the particles start to move as one collective and that the size of the largest cluster grows with time as more particles join the largest cluster. This algorithm is a generalisation of the one used in the milling paper as we can reproduce the original algorithm used by setting  $\text{minPts} = 1$  and  $\epsilon = 0.5$ .

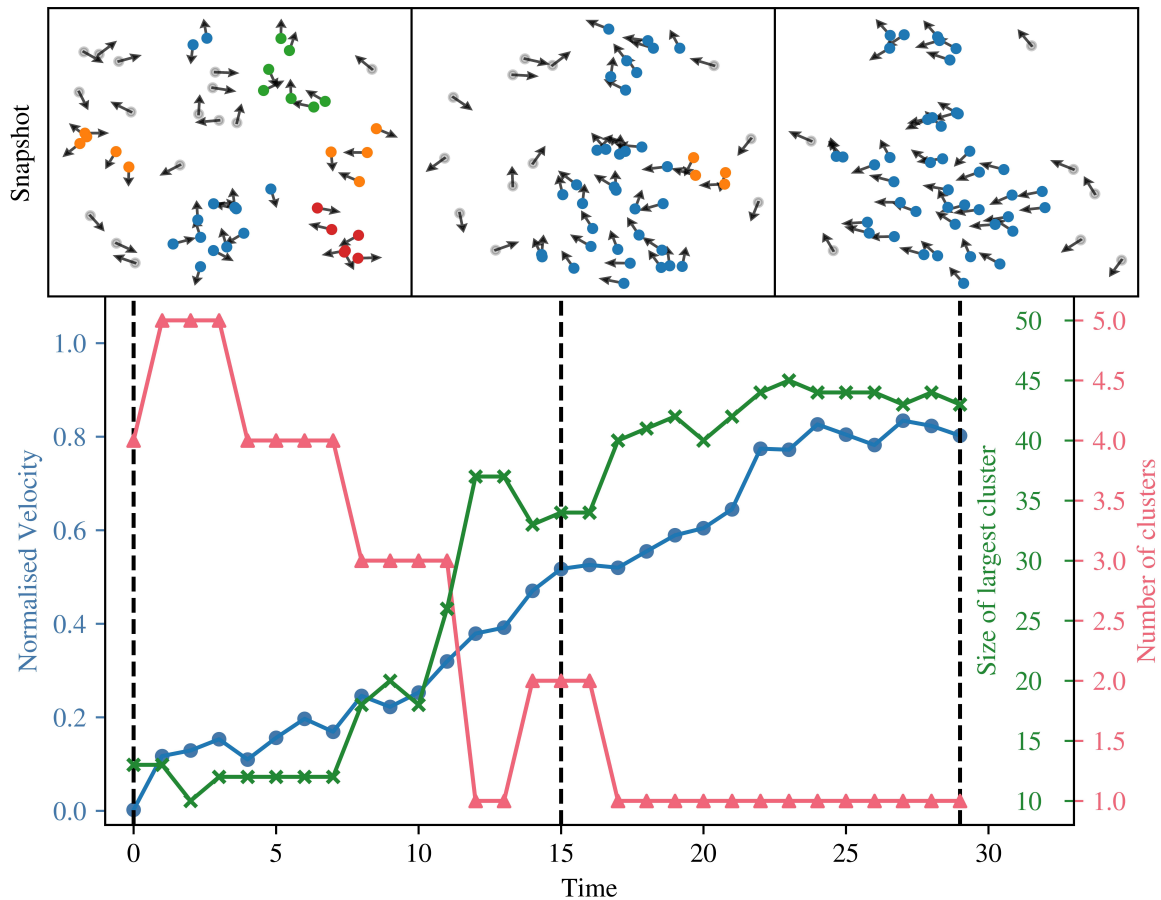


**FIG. 15:** Evolution of the order parameter and clustering statistic for the original Vicsek model. Snapshots show the state of the system at the time indicated by the black dotted lines. The colour of the particles distinguish clusters, with grey points representing the noise points. For the parameters:

$$v = 0.3, L = 5, N = 50, \eta = 2.0, \text{minPts} = 4 \text{ and } \epsilon = 0.5$$

## 6.2. Vortex Criteria

To check if a given cluster is a vortex we compute the normalised angular momentum  $m_a$  using

$$m_a = \frac{1}{N} \sum_{i=1}^N \frac{|\mathbf{r}_{\text{CM},i} \times \mathbf{u}_i|}{|\mathbf{r}_{\text{CM},i}|} \quad (6)$$

where  $\mathbf{r}_{\text{CM},i}$  is the vector from the center of mass of the cluster to the  $i$ -th particle and  $\mathbf{u}_i$  is the velocity unit vector of the  $i$ -th particle. This is 0 when no particles in the cluster are rotating around the center of mass and 1 when all particles in the cluster are rotating around the center of mass. We follow the criteria from the milling paper to classify vortices, such that a cluster is a vortex if  $m_a > 0.75$  and  $v_a < 0.5$ . This identifies the vortices from other configurations such as the flocks and bands of the system [6].

## 6.3. Problems With Existing Methods

One problem with the original algorithm ( $\text{minPts} = 1$  and  $\epsilon = 0.5$ ) proposed in the milling paper is highlighted Fig. 16. We observe in 16(a) and 16(b) the existence of short lived false positive vortices. The mechanism for the formation of these is illustrated in Fig. 17(a). False positives occur in the situation where particles with opposite velocity form a cluster. These configurations have low normalised velocity and high normalised angular momentum fulfilling the vortex detection criteria. This is most prominent where we have high noise, with the particles undergoing diffusion as shown in Fig. 16(b).

False positives can be removed by increasing the  $\text{minPts}$  parameter in the DBSCAN algorithm. Noise points are not considered for vortex detection hence increasing the minimum size of clusters reduces the likelihood of false positives occurring. This confirms the results we observe in Fig. 16(c) and 16(d). Increasing  $\text{minPts}$  reduces false positives however if this value is too large then the algorithm will fail to detect a real vortex causing a false negative.

We observe the appearance of false negatives in Fig. 16(a) and 16(c). We can visually confirm more vortices than the algorithm detects. The configuration that produces this error is shown in Fig. 17(b). The many particles outside the vortex pulls the center of mass away from the center of the vortex distorting the clustering statistics. The DBSCAN algorithm cannot identify these false negatives. These problems were not considered in the original milling paper as their experiments were not concerned with tracking vortex formation over time.

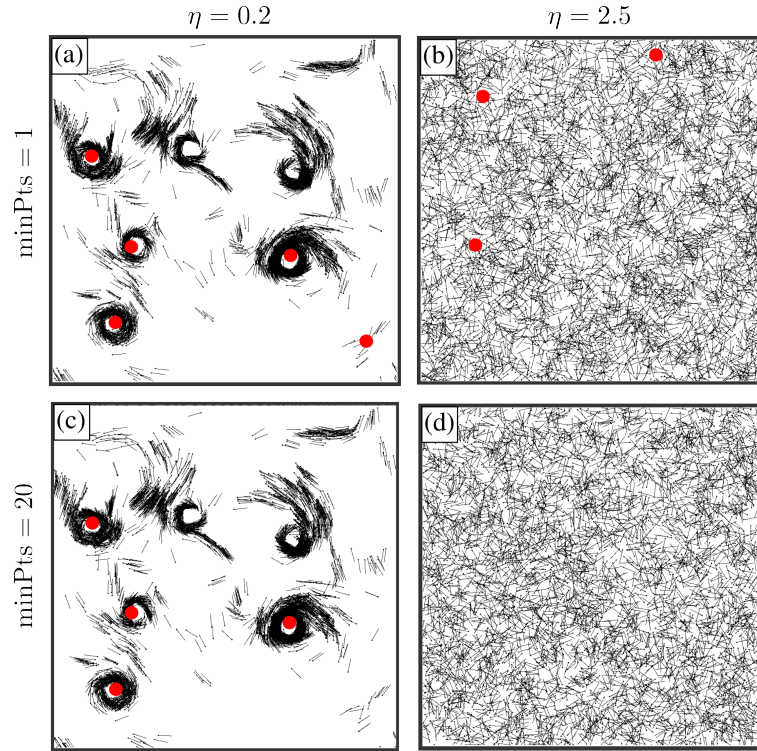


**FIG. 16:** Comparison of the vortex detection algorithm for different values of  $\text{minPts}$  and noise. The red circles represent where the algorithm has identified a vortex being formed. Parameters:  $v = 0.1$ ,  $L = 25$ ,  $N = 5000$ ,  $\phi = 180^\circ$ ,  $\omega = 10^\circ$ ,  $\epsilon = 0.5$

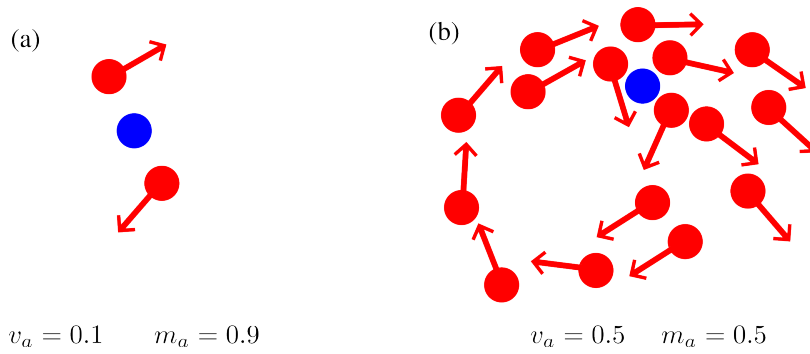


**FIG. 17:** Problematic cluster configurations for the original vortex detection algorithm. Red arrows represent the direction of travel for the particles and blue circles represent the center of mass of the cluster. (a) Opposite moving particles forming a false positive (b) Large cluster with embedded vortex forming a false negative.

#### 6.4. New Vortex Detection Algorithm

To remove the false negatives of the type shown in Fig. 17(b) we develop a new algorithm for vortex detection. The main principle behind this algorithm is illustrated in Fig. 18. For each particle we store the positions of the previous three time steps 18(a). A unique circle of radius  $r_{CR}$  can be constructed from the three historic positions giving a center of rotation 18(b). For milling configurations the centers of rotations of the particles will cluster together 18(c).

Particles moving in a straight line (not milling) will have very large  $r_{CR}$  which we can ignore. We use the DBSCAN algorithm to cluster the remaining centers of rotation. It was empirically found that  $\text{minPts} = 20$  and  $\epsilon = 0.1$  provided accurate classification of the vortices. Further we check normalised velocity and normalised angular momentum of the particles forming the cluster to ensure that the clusters satisfy the vortex criteria. To prevent the classification of false positives we store the history of the centers of mass of the valid clusters for 20 time steps and perform clustering on this data with  $\text{minPts} = 5$  and  $\epsilon = 0.1$ . Empirically clustering on the history of valid vortices with these parameter values prevented false positives occurring.

The flow diagram of this algorithm is shown in Fig. 19 (a). We ignore particles with  $r_{CR}$  greater than half the box length as we do not expect vortices of this size to form. The comparison between the simple DBSCAN algorithm and the new vortex detection algorithm is shown in Fig. 19(b) and 19(c) respectively. We observe that the new algorithm classifies the false negatives of 19(b). The new algorithm has the ability to track vortex formation over time however due to the more complicated nature of the algorithm the computational complexity has increased.

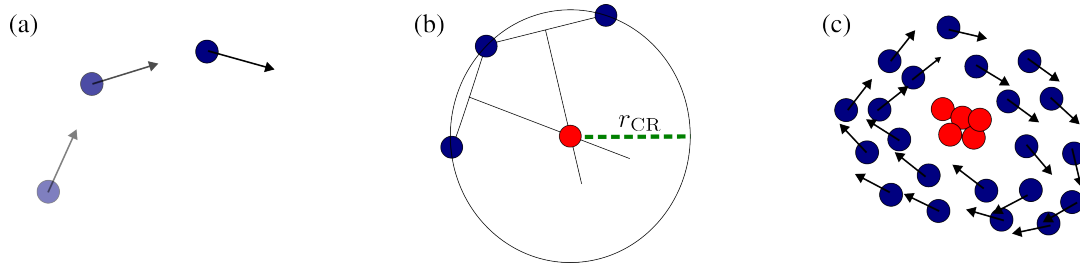


**FIG. 18:** Visualisation of the new vortex detection algorithm. (a) The previous 3 positions of a particle with the more historic particles being indicated by increasing transparency (b) The unique circle through the three points with the center of rotation highlighted in red and the radius highlighted in green (c) Example of the formation of the center of rotation cluster for a milling state.

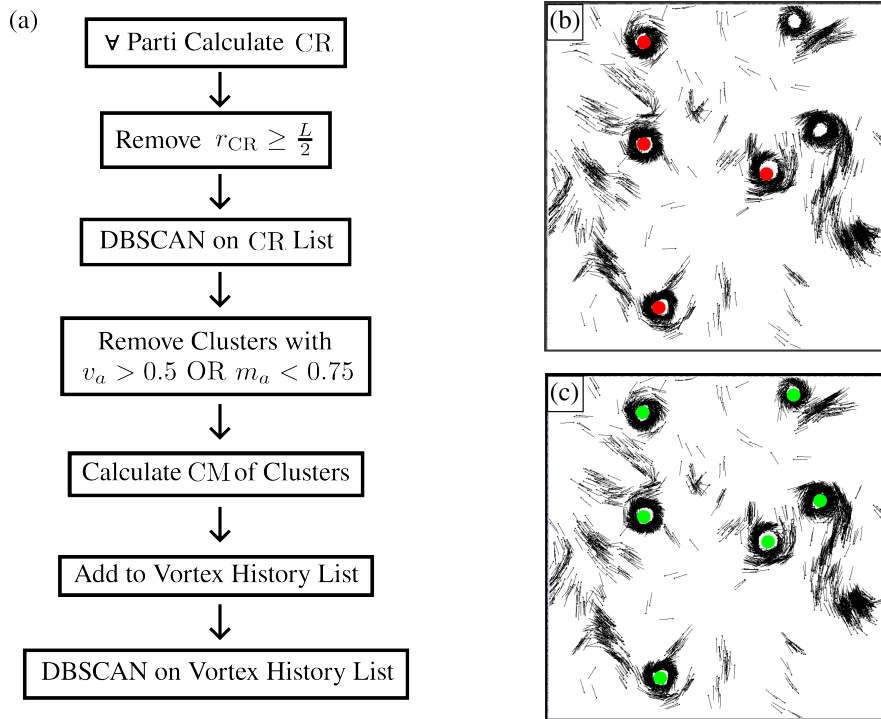


**FIG. 19:** (a) The flow diagram of the new vortex detection algorithm (full explanation in text) (b) Simple DBSCAN vortex detection using  $v = 0.1$ ,  $L = 25$ ,  $N = 5000$ ,  $\eta = 0.2$ ,  $\phi = 180^\circ$ ,  $\omega = 10^\circ$ ,  $\text{minPts} = 20$ ,  $\epsilon = 0.5$  with the red circles indicating a detected vortex (c) The new vortex detection algorithm for the same parameters with the green circles indicating a detected vortex.

## 7. MILLING EXPERIMENTS

### 7.1. Results

The effect of the milling regime on the normalised velocity is illustrated in Fig. 20. We compare this to the original Vicsek model in which the normalised velocity increases over time as the system becomes more ordered. The modifications introduce a different initial region in which vortices are formed. Successful vortex formation requires the normalised velocity to be small hence when a large proportion of the system is undergoing milling we expect the normalised velocity to be closer to zero. Unstable vortices existing for around 10 time steps arise from collisions of clusters and are observed as sharp peaks in the number of vortices. We observe collective motion of the original Vicsek type after the milling region has dissolved.

Vortex statistics can be obtained by considering the number of vortices formed over time. Given the random initial configuration of positions and velocities it is never guaranteed that the system achieves milling. We define  $P_{\text{mill}}$  to be the proportion of runs in which milling is achieved. To compute  $P_{\text{mill}}$  we repeat experiments 100 times and count the number of times milling systems are produced. We observe in Fig. 20 that the maximum number of vortices formed is four. We can calculate the average maximum number of vortices produced across the 100 repeats, this indicates how conducive the system is to vortex formation. Further we can track the time step of the last detected vortex which gives indication of the stability of the vortices in the system, in Fig. 20 this is 387.

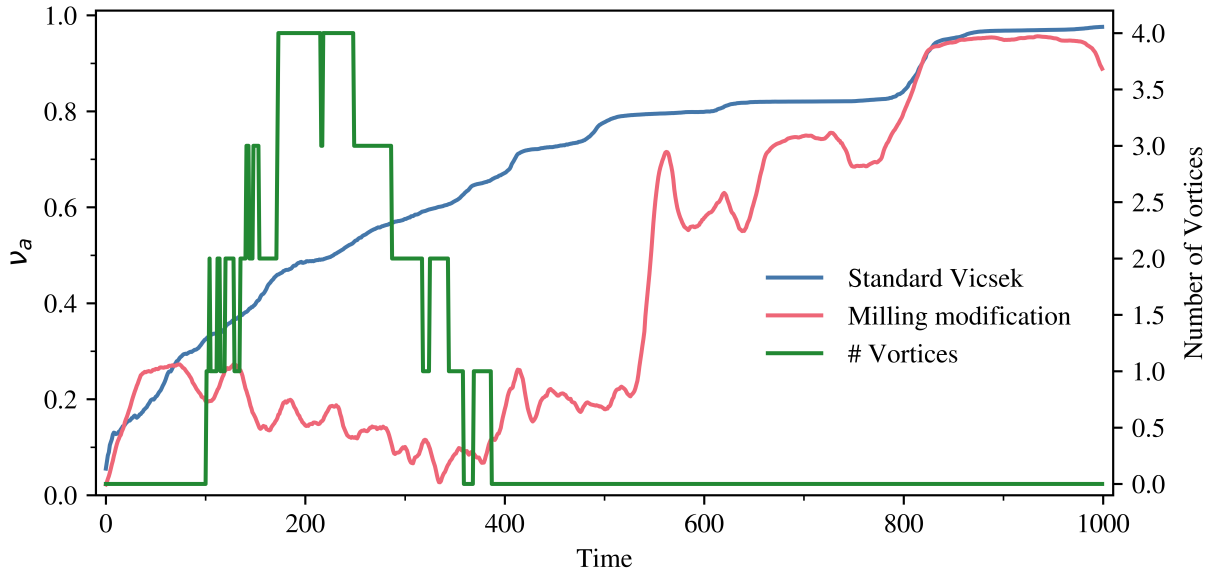


**FIG. 20:** The evolution of the normalised velocity for the non-milling Vicsek model ( $\phi = 360^\circ$  and  $\omega = 180^\circ$ ) and milling model ( $\phi = 180^\circ$  and  $\omega = 10^\circ$ ). The number of vortices in the milling model is highlighted. For parameters:  $v = 0.1$ ,  $L = 35$ ,  $N = 7000$ ,  $\eta = 0.1$ .

In the same manner as the standard Vicsek model the modified model has behaviour dependent on noise. As opposed to the transition between disorder and order, decreasing noise can transition a disordered regime into a milling regime. We observe such a transition in Fig. 21(a). The milling proportion increases as we decrease noise implying that the milling regime has higher stability at lower noise. This transition appears at smaller noise values than the order-disorder transition of the standard Vicsek model.

We note the correlation between all the vortex statistics. We observe an unexpected peak in the last vortex observed just after the transition. Given the large error of this data we cannot make definite conclusions however we suggest that this is caused by the larger random motion of the particles at the transition boundary being able to form unstable vortices much later than in other systems.

The difference in configuration of the ordered clusters between the Vicsek and the modified model is shown in Fig. 21(b) and 21(c) respectively. These are the clusters formed in the long time limit of Fig. 20. The restricted field of view of the modified model creates longer dart like clusters compared to the rounder clusters found in the original model. In milling regimes there is a coexistence between these dart and milling clusters.

The density dependence of the milling regime is presented in Fig. 22. We observe that as density is increased the chance of milling occurring increases. The average maximum number of mills increases as we increase the number of particles. Furthermore, we observe vortices at a larger time step by increasing the number of particles.

The dependence of the milling regime on the field of view and maximum angular velocity is shown in Fig. 23. In agreement with original milling paper we observe vortices formed at  $\phi \sim 200^\circ$  and  $\omega \sim 10^\circ$  [6]. We note the agreement with Fig. 22 at the maximal  $P_{\text{mill}}$ . We expect the maximum angular velocity to depend on the particle velocity and we observe under the same conditions a larger particle speed dampens the milling regime.

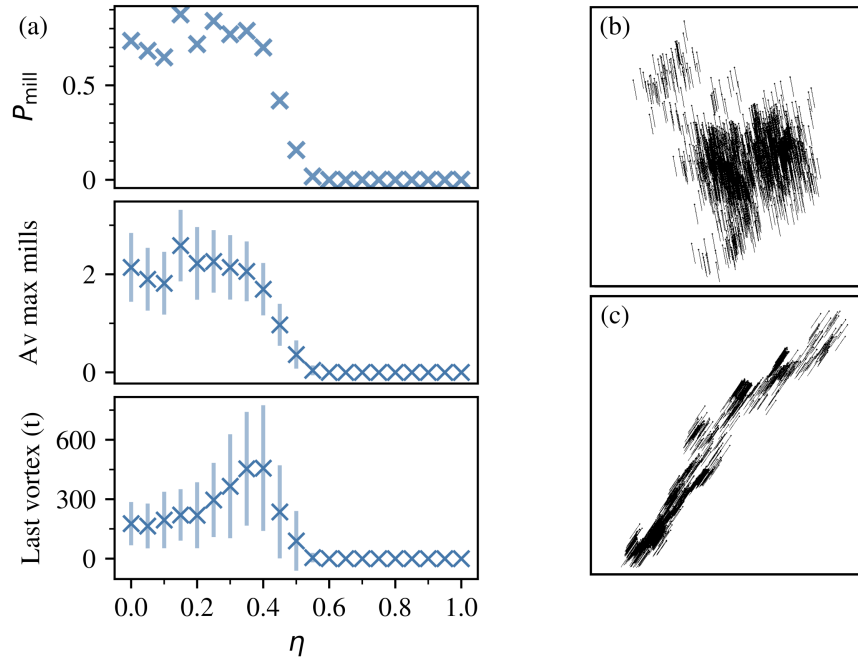


**FIG. 21:** (a) The noise dependence on the milling regime for  $v = 0.1$ ,  $L = 20$ ,  $N = 2000$ ,  $\phi = 180^\circ$  and  $\omega = 10^\circ$  (b) Ordered cluster for  $\eta = 0.0$ ,  $\phi = 360^\circ$  and  $\omega = 180^\circ$  (c) Ordered cluster for  $\eta = 0.0$ ,  $\phi = 180^\circ$  and  $\omega = 10^\circ$ .

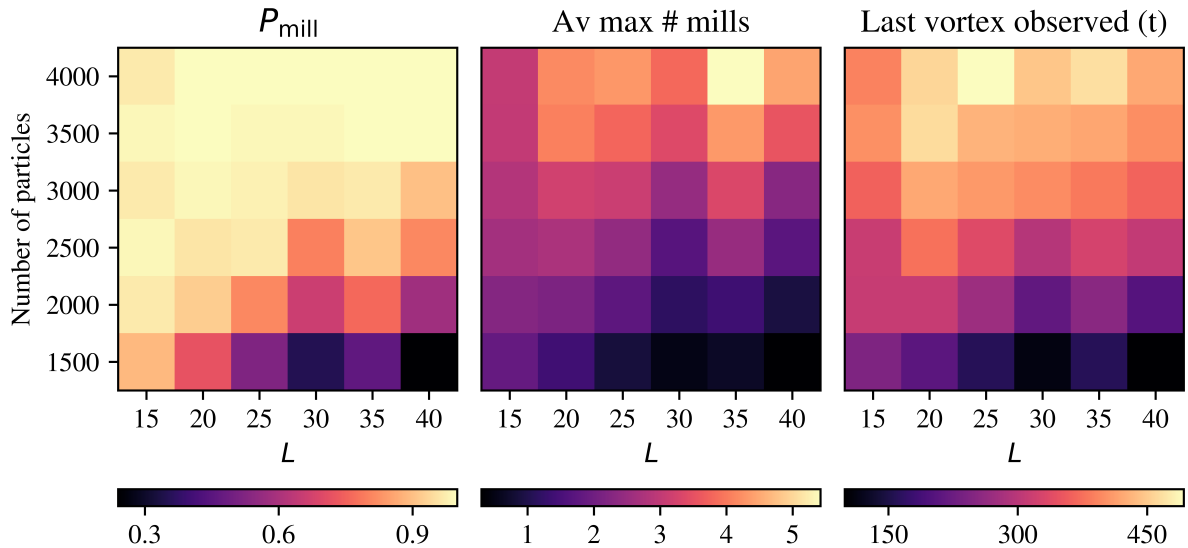


**FIG. 22:** Heat maps of the effect of density on the milling regime. For parameters  $v = 0.1$ ,  $\eta = 0.0$ ,  $\phi = 180^\circ$ ,  $\omega = 10^\circ$  for 1000 time steps.

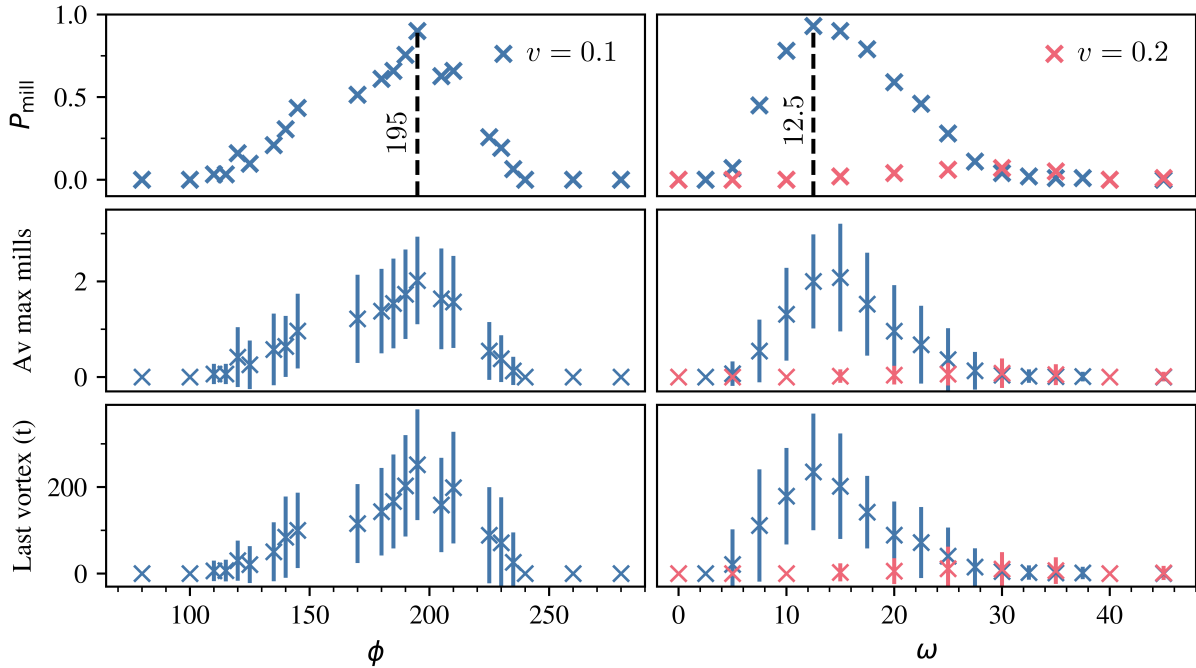


**FIG. 23:** The dependence of the milling regime on the field of view (at  $\omega = 10^\circ$ ) and maximum angular velocity (at  $\phi = 180^\circ$ ) for two speeds of particles with maximal values of  $P_{\text{mill}}$  highlighted.

For parameters  $L = 20$ ,  $N = 2000$ ,  $\eta = 0.0$ .

## 7.2. Discussion

In general there is an interdependence between the parameter values and the regimes formed by the model. The two additional parameters of the modified model increase the complexity of the relation between the model and the parameters. An instance of this can be observed by the more complex formations of particles such as vortices and darts (see Fig. 21(c)). We do not explore the relationship between parameters and regimes in detail due to time constraints. However we discuss the general trends of the parameters in relation to the milling regime.

We observe that a decrease in noise creates a transition from a disordered regime to a milling regime. Vortex formation occurs when the constituent particles are rotating at approximately the maximum angular velocity [6]. A sufficiently large noise term will disrupt the alignment necessary for rotating hence the observation that  $P_{\text{mill}}$  decreases as noise increases as shown in Fig. 21. The relation between noise and maximum angular velocity explains why the transition occurs at lower noises than the original Vicsek transition.

A greater density increases the chance of the formation of vortices as shown in Fig. 22. Given the same probability of forming a vortex increasing the number of particles will increase the number of vortices observed. The greater number of vortices observed will also correlate to the final vortex observed as there is a higher chance for a longer lasting vortex to form.

Particles will only form vortices if they cannot align to particles behind them and they have a sufficiently large field of view given a maximum angular velocity. This explains the range of field of view in Fig. 23. The maximum angular velocity and the speed of the particles are related as the speed at which the particles must turn to stay in the vortex is dependent on how far they move in a given time step.

Our results reproduce the general trends found in the original milling paper (Ref. [6]). The construction of a new vortex detection algorithm allowed for the reliable tracking of vortex formation across time which was not possible in previous implementations. This algorithm can be applied to explore vortex formation in other active matter systems.

The true behaviour of systems found in nature, such as schools of fish, show more complicated configurations such as elliptical milling. These formations can be explained with the use of more complicated models. The current best understanding for these formations involves using models with attraction and repulsion zones alongside field of view and maximum angular rotation parameters [7].

## 8. CONCLUSIONS

In this paper we explored the phase transition of the Vicsek model, a simple model used to describe collective motion in active matter systems. We have provided computational methods for the production of large simulations and have built an application to simulate the model in real time. These techniques were used to analyse the trends of the phase transition presented by varying the noise and density and our findings are in agreement with the literature. Furthermore, we show the presence of band formation indicative to the liquid-gas nature of the phase transition.

We modified the Vicsek model to study the phenomena of milling states commonly found in nature. We have improved upon the existing vortex detection algorithm and provided a new algorithm for real time tracking of vortex formation. Using the techniques developed we explored how the vortex formation depends on the model parameters with our findings in agreement with the literature.

These models are minimal and are too simplistic to accurately describe behaviour found in nature however they act as a basis for further exploration into more realistic models. The real time simulation developed could be of interest in teaching and understanding collective motion and the new vortex detection algorithm could have applications in other active matter simulations.

## 9. FUTURE WORK

The simulation application could be extended to explore the nature of the bands in the liquid-gas phase transition. The details of the fluid band structure illustrated in Fig. 11 were outside the current scope of the application. Improved efficiency of updating algorithms and the use of larger computing resources could illuminate this region further.

A more detailed study of the peak of the last vortex detected in Fig. 21(a) would allow more reliable conclusions to be drawn about the mechanism causing this phenomena. Further research could extend the efficiency of the new vortex detection algorithm and apply this method to other collective motion simulations.

## REFERENCES

- [1] G. De Magistris and D. Marenduzzo, “An introduction to the physics of active matter,” *Physica A*, vol. 418, pp. 65–77, 2015.
- [2] É. Fodor and M. Cristina Marchetti, “The statistical physics of active matter: From self-catalytic colloids to living cells,” *Physica A*, vol. 504, pp. 106–120, 2018.
- [3] T. Vicsek, A. Czirók, E. Ben-Jacob, I. Cohen, and O. Shochet, “Novel type of phase transition in a system of self-driven particles,” *Phys. Rev. Lett.*, vol. 75, no. 6, pp. 1226–1229, 1995.
- [4] P. Chatterjee, “The Flocking Transition : A Review of The Vicsek Model,” 2017.
- [5] A. P. Solon, H. Chaté, and J. Tailleur, “From phase to microphase separation in flocking models: The essential role of nonequilibrium fluctuations,” *Phys. Rev. Lett.*, vol. 114, p. 068 101, 6 2015.
- [6] A. Costanzo and C. K. Hemelrijk, “Spontaneous emergence of milling (vortex state) in a vicsek-like model,” *Journal of Physics D*, vol. 51, no. 13, p. 134 004, 2018.
- [7] T. Vicsek and A. Zafeiris, “Collective motion,” *Physics Reports*, vol. 517, no. 3-4, pp. 71–140, 2012.
- [8] G. Grégoire and H. Chaté, “Onset of collective and cohesive motion,” *Phys. Rev. Lett.*, vol. 92, p. 025 702, 2 2004.
- [9] A. Onuki, *Phase Transition Dynamics*. Cambridge University Press, 2002.
- [10] F. Ginelli, “The physics of the vicsek model,” *The European Physical Journal Special Topics*, vol. 225, no. 11-12, pp. 2099–2117, 2016.
- [11] W. Bugden and A. Alahmar, *Rust: The programming language for safety and performance*, 2022. arXiv: 2206.05503.
- [12] *Stack Overflow Developer Survey 2022*. [Online]. Available: [https://survey.stackoverflow.co/2022/?utm\\_source=social-share&utm\\_medium=social&utm\\_campaign=dev-survey-2022](https://survey.stackoverflow.co/2022/?utm_source=social-share&utm_medium=social&utm_campaign=dev-survey-2022) (visited on 04/05/2023).
- [13] S. Alavi, *Molecular Simulations: Fundamentals and Practice*. Jun. 2020, ISBN: 9783527699452.
- [14] *Ggez: Rust game thing*. [Online]. Available: <https://ggez.rs/> (visited on 04/06/2023).
- [15] P. Novak, *Pn2200/g3data*, Jan. 2023. [Online]. Available: <https://github.com/pn2200/g3data> (visited on 04/06/2023).
- [16] H. Chaté, F. Ginelli, G. Grégoire, and F. Raynaud, “Collective motion of self-propelled particles interacting without cohesion,” *Phys. Rev. E*, vol. 77, p. 046 113, 4 2008.
- [17] M. Ester, H.-P. Kriegel, J. Sander, and X. Xu, “A density-based algorithm for discovering clusters in large spatial databases with noise,” in *Knowledge Discovery and Data Mining*, 1996.